JACS
JOURNAL OF THE AMERICAN CHEMICAL SOCIETY
Communication
pubs.acs.org/JACS

Modeling TauD-*J*: A High-Spin Nonheme Oxoiron(IV) Complex with High Reactivity toward C−H Bonds

Achintesh N. Biswas,[†] Mayank Puri,[†] Katlyn K. Meier,[‡] Williamson N. Oloo,[†] Gregory T. Rohde,[†] Emile L. Bominaar,*[,‡] Eckard Münck,*[,‡] and Lawrence Que, Jr.*[,†]

[†]Department of Chemistry and Center for Metals in Biocatalysis, University of Minnesota, Minneapolis, Minnesota 55455, United States

[‡]Department of Chemistry, Carnegie Mellon University, Pittsburgh, Pennsylvania 15213, United States

Supporting Information

ABSTRACT: High-spin oxoiron(IV) species are often implicated in the mechanisms of nonheme iron oxygenases, their C−H bond cleaving properties being attributed to the quintet spin state. However, the few available synthetic $S = 2$ Fe^{IV}=O complexes supported by polydentate ligands do not cleave strong C−H bonds. Herein we report the characterization of a highly reactive $S = 2$ complex, $[Fe^{IV}(O)(TQA)(NCMe)]^{2+}$ (**2**) (TQA = tris(2-quinolylmethyl)amine), which oxidizes both C−H and C=C bonds at −40 °C. The oxidation of cyclohexane by **2** occurs at a rate comparable to that of the oxidation of taurine by the TauD-*J* enzyme intermediate after adjustment for the different temperatures of measurement. Moreover, compared with other $S = 2$ complexes characterized to date, the spectroscopic properties of **2** most closely resemble those of TauD-*J*. Together these features make **2** the best electronic *and* functional model for TauD-*J* to date.

High-spin oxoiron(IV) species have been trapped and characterized as key intermediates in the dioxygen activation mechanisms of mononuclear nonheme iron enzymes[1] by the seminal efforts of Bollinger and Krebs.[2] A related species is proposed to be the oxidant formed in the reactions of N_2O with coordinately unsaturated iron(II) centers in carboxylate-based metal−organic frameworks that catalyze ethane hydroxylation.[3] The quintet ($S = 2$) species is predicted by density functional theory (DFT) calculations to be more reactive in H atom transfer (HAT) than the corresponding triplet ($S = 1$) species.[4] In particular, Shaik has emphasized the role of exchange to stabilize the high-spin Fe^{III}−OH transition state in HAT by high-spin $Fe^{IV}(O)$ complexes.[4e]

These developments have fueled a significant synthetic effort that has led to the characterization of over 60 oxoiron(IV) complexes in the past decade.[5] However, most of these complexes have triplet ground states, and only a handful possess a quintet ground state. One successful strategy to obtain $S = 2$ Fe^{IV}=O complexes has been to employ sterically bulky tripodal ligands that enforce a trigonal-bipyramidal geometry on the iron(IV) center,[6,7] but these complexes exhibit rather sluggish intermolecular reactivity, perhaps because of steric constraints. An alternative strategy to obtain $S = 2$ Fe^{IV}=O complexes is to use a weaker-field ligand environment than that provided by the tertiary amine/N-heterocycle combinations used to date. Bakac and co-workers have shown that the $S = 2$ $[Fe^{IV}(O)(H_2O)_5]^{2+}$ ion can be obtained in acidic aqueous solution and is in fact highly reactive,[8] but its short lifetime ($t_{1/2} \sim 20$ s at 25 °C) has made its detailed characterization challenging. We have thus sought to identify a tripodal ligand with weaker-field donors that would allow the trapping of a sterically less hindered $S = 2$ Fe^{IV}=O species that would exhibit higher reactivity. Herein we report the synthesis and characterization of the $S = 2$ complex $[Fe^{IV}(O)(TQA)]^{2+}$ (**2**) (TQA = tris(2-quinolylmethyl)amine), with weaker-field quinolines[9] replacing the pyridines of the popular TPA ligand. Complex **2** exhibits spectroscopic properties distinct from $[Fe^{IV}(O)(TPA)(NCCH_3)]^{2+}$[10] and remarkably higher reactivity toward alkanes and alkenes.

The reaction of TQA and $Fe^{II}(OTf)_2(CH_3CN)_2$ in CH_3CN affords $[Fe^{II}(TQA)(OTf)_2]$ (**1**). Its crystal structure shows a six-coordinate high-spin iron(II) center (Figure 1 left and Tables S1 and S2). Treatment of **1** with 2-(^{t}BuSO$_2$)C$_6$H$_4$IO (ArIO)[11] at −40 °C leads to the formation of a highly reactive intermediate **2** that has a half-life of 15 min and exhibits a near-UV shoulder at 400 nm and weak bands at 650 nm ($\varepsilon_M = 300$ M^{-1} cm^{-1}) and 900

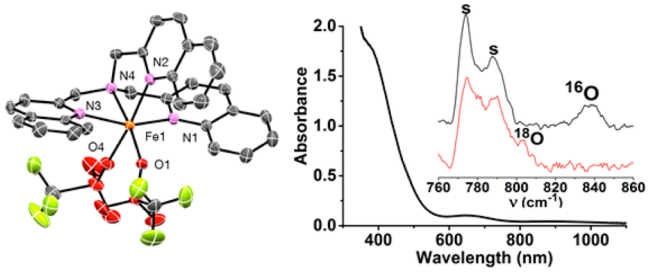

Figure 1. (left) ORTEP plot for $[Fe^{II}(TQA)(OTf)_2]$ (**1**) with 50% probability ellipsoids and H atoms omitted for clarity. Selected bond lengths (Å): Fe(1)−N(1), 2.2155(17); Fe(1)−N(2), 2.2308(17); Fe(1)−N(3), 2.1954(17); Fe(1)−N(4), 2.1748(17); Fe(1)−O(1), 2.0450(14); Fe(1)−O(4), 2.1965(15). (right) UV−vis spectrum of **2** from the reaction of 0.4 mM **1** with 2 equiv of ArIO in CH_3CN at −40 °C. Inset: resonance Raman spectra ($\lambda_{ex} = 514.5$ nm, 60 mW power) of [^{16}O]**2** (top) and [^{18}O]**2** (bottom) in frozen CH_3CN solution. (Off-resonance excitation was used to minimize the effects of photoreduction.[6a])

Received: November 15, 2014
Published: February 12, 2015

DOI: 10.1021/ja511757j
J. Am. Chem. Soc. 2015, 137, 2428−2431

Table 1. Properties of Synthetic $[Fe^{IV}(O)L]$ Complexes[a]

L	TQA	TPA	Me_3NTB	TMG_3tren	$(H_2O)_5$	TauD-*J*
λ_{max} (nm)	400(sh), 650, 900	724	380, 770	400, 825, 866		~318
S	2	1	1	2	2	2
D (cm^{-1})	17(1)	28	28	5.0	9.7	10.5
ΔE_Q (mm/s)	−1.05(2)	0.92	1.53	−0.29	−0.33	−0.90
$A_{x,y}/g_n\beta_n$ (T)	−18.2(4), −16.6(4)	−23.5	−19.0	−15.5	−20.3	−18.4, −17.6
$A_z/g_n\beta_n$ (T)	-31.7^b	−5.0	0	−28.0	–	−31.0
δ (mm/s)	0.24(2)	0.01	0.02	0.09	0.38	0.30
ref	this work	10	12	6a	8	2c

[a]Abbreviations used: Me_3NTB = tris(1-methylbenzimidazol-2-ylmethyl)amine, TMG_3tren =1,1,1-tris{2-[N^2-(1,1,3,3-tetramethylguanidino)]ethyl}-amine. [b]$A_z/g_n\beta_n(T)$ could not be determined experimentally for **2** and was estimated from calculations described below.

nm (ε_M = 75 M^{-1} cm^{-1}) (Figure 1 right). Its properties suggesting the formation of an Fe^{IV}═O complex are compared with those of others in Table 1. A resonance-enhanced Raman vibration is found at 838 cm^{-1}, which shifts to 803 cm^{-1} upon ^{18}O-labeling of **2**, as expected for the ν(Fe═O) mode. Electrospray ionization mass spectrometry (ESI-MS) analysis of **2** supports its formulation as $[Fe^{IV}(O)(TQA)]^{2+}$, with a peak observed at *m*/*z* 256.1. However, the isotope distribution pattern suggests contamination with $[Fe^{III}(OH)(TQA)]^{2+}$ (*m*/*z* 256.6) due to the instability of **2** (Figure S1 in the SI). Indeed, the dominant feature in its ESI-MS spectrum is a peak at *m*/*z* 662 that corresponds to $[Fe^{III}(OH)(TQA)(O_3SCF_3)]^+$. Also present is a peak at *m*/*z* 676 that corresponds to $\{[Fe^{III}(OH)(TQA)(OTf)] + O - 2H\}^+$, suggesting the oxidation of one TQA CH_2 group to a carbonyl.

Figure 2 shows 4.2 K Mössbauer spectra of **2** recorded at various applied fields; additional spectra are shown in Figure S2.

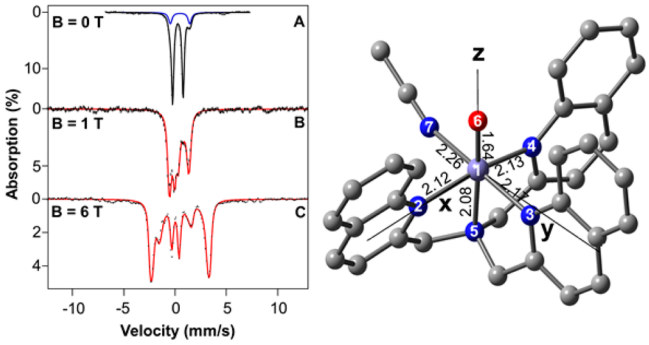

Figure 2. (left) Mössbauer spectra recorded at 4.2 K in parallel applied magnetic fields as indicated. The blue line in (A) outlines a diiron(III) contaminant (12% of Fe). We have subtracted the spectra of this contaminant from the data in (B) and (C). A second contaminant, a high-spin Fe(III) species (18%), has been removed in (B) and (C); details are given in the SI. For the spectral simulations for **2** (red lines), we employed the software WMOSS for the *S* = 2 spin Hamiltonian $\hat{H} = D[\hat{S}_z^2 - 2 + (E/D)(\hat{S}_x^2 - \hat{S}_y^2)] + 2\beta\hat{\mathbf{S}}\cdot\mathbf{B} + \hat{\mathbf{S}}\cdot\mathbf{A}\cdot\hat{\mathbf{I}} - g_n\beta_n\mathbf{B}\cdot\hat{\mathbf{I}} + (eQV_{zz}/12)[3\hat{I}_z^2 - 15/4 + \eta(\hat{I}_x^2 - \hat{I}_y^2)]$ using the parameters listed in Table 1 and *n* = 0. (right) Geometry-optimized structure of **2** in the gas phase with Fe−ligand distances shown.

The zero-field spectrum exhibits a quadrupole doublet (~70% of Fe) with splitting ΔE_Q = −1.05 mm/s and isomer shift δ = 0.24 mm/s. The remainder of the Fe in the sample belongs to high-spin Fe(III) decay products, 18% representing mononuclear Fe(III) that presumably corresponds to the $[Fe^{III}(OH)(L)]^{2+}$ species observed in the ESI-MS spectrum (Figure S1) and 12% from a diferric complex (ΔE_Q = +1.90 mm/s, δ = 0.45 mm/s; blue line in Figure 2A). By means of spectral simulations (shown in Figure S3) these contaminants were subtracted from the raw data to yield the spectra in Figures 2B,C and S2. The isomer shift of **2** is quite positive compared with values for other oxoiron(IV) complexes supported by polypyridine ligands,[12,13] suggesting that this species is a high-spin iron(IV) complex. This spin-state assignment is strongly supported by analysis of the magnetic hyperfine structure. The spectra of **2** exhibit increased magnetic hyperfine splittings with increasing applied field. This increase follows a "magnetization" curve with a shape determined by the magnitude of the zero-field splitting parameter *D*. From spectral simulations using an *S* = 2 spin Hamiltonian (red lines in Figures 2 and S2) we obtained the parameters listed in Table 1. Simulating the spectra for *S* = 1 would require $A_{x,y}/g_n\beta_n$ to be (−33, 32) T, which is unreasonably large compared with the typical $A_{x,y}/g_n\beta_n$ = (−21, 21) T,[14] ruling out the *S* = 1 assignment. Table 1 shows that the magnetic hyperfine parameters previously reported for TauD-*J* are best reproduced by **2**, making it the best spectroscopic model for TauD-*J* to date.

The change in spin state in going from $[Fe^{IV}(O)(TPA)(NCMe)]^{2+}$ (*S* = 1) to **2** (*S* = 2) can be rationalized by an earlier study on Fe(TPA) complexes.[9a] Lower spin states could be attained for Fe^{II} and Fe^{III} complexes of the parent TPA ligand but became less likely as the number of pyridine α-substituents increased because of steric interactions involving the α-C−H bonds, which prevent formation of the shorter Fe−N_{py} bonds required by a lower-spin iron center.[9a] For the oxoiron(IV) series, *S* = 1 complexes were obtained for TPA and derivatives with one α-substituent.[9b] However, with all three pyridine donors having α-substituents, TQA is not able to support an *S* = 1 Fe^{IV}═O center and instead gives rise to an *S* = 2 Fe^{IV}═O complex. The principle for this design strategy is supported by a computational comparison of several structures related to TQA (see pp S14−S16 in SI for additional details).

The right panel of Figure 2 shows the DFT-optimized geometry of **2**, formulated as $[Fe^{IV}(O)(TQA)(NCMe)]^{2+}$, obtained using Gaussian 09 (Table S3). The calculations yielded ΔE_Q = −1.14 mm/s, η = 0.34 ($0 \le \eta_{exp} < 0.3$), and δ = 0.24 mm s^{-1}, in excellent agreement with the experimental data.[15] The validity of two alternative formulations for **2** was also assessed by DFT. Five-coordinate $[Fe^{IV}(O)(TQA)]^{2+}$ was ruled out, as it yielded a δ of 0.15 mm s^{-1} that was inconsistent with experiment, but $[Fe^{IV}(O)(TQA)(OTf)]^+$ gave rise to the same isomer shift as predicted for $[Fe^{IV}(O)(TQA)(NCMe)]^{2+}$ and observed experimentally (Table S3). To distinguish between the two six-coordinate formulations, a ^{19}F NMR study of **2** was performed at −40 °C, which revealed only one peak at −80 ppm, the same chemical shift as for free triflate (Figures S8−S13). This peak represents all of the triflate in the sample and has a line width 5-fold broader than that found for free triflate. When these

DOI: 10.1021/ja511757j
J. Am. Chem. Soc. 2015, 137, 2428−2431

observations are judged against the data accumulated in Table S6, we surmise that only a small fraction of the triflate binds to the $Fe^{IV}(O)$ unit and is in rapid equilibrium with unbound triflate, making $[Fe^{IV}(O)(TQA)(OTf)]^+$ a minor component of **2** in MeCN solution. Thus, taking the ^{19}F NMR and DFT results together, we conclude that **2** is best formulated as $[Fe^{IV}(O)(TQA)(NCMe)]^{2+}$.

The DFT-calculated spin-dipolar contribution to the ^{57}Fe magnetic hyperfine tensor is $A_{x,y,z(s\text{-}d)}/g_n\beta_n$ = (+3.0, +6.5, −9.5) T. We estimated $A_{iso} = (A_x + A_y + A_z)/3$ from the experimental values $A_x/g_n\beta_n$ = −18.2 T, $A_y/g_n\beta_n$ = −16.6 T by using the calculated spin-dipolar values along *x* and *y*, obtaining for the contact term $A_c/g_n\beta_n \sim A_{iso}/g_n\beta_n$ = −22.2 T (as shown in the SI, the *g* values of **2** are estimated as $g_x = g_y \approx 1.98$ and $g_z = 2.00$, and therefore, the orbital contributions to **A** are expected to be quite small). We then obtained $A_z/g_n\beta_n$ = −31.7 T from $A_{iso} + A_{z(s\text{-}d)}$. The entries in Table 1 reveal that the parameters of **2** are quite close to those reported for TauD-***J***. As shown on p S13 in the SI, the predominant contribution to the *D* value of **2** arises from spin−orbit coupling between the *S* = 2 ground state and a low-lying (~2700 cm^{-1}) *S* = 1 excited state. This is also the case for TauD-***J***, and its smaller *D* value suggests that its *S* = 1 state has a higher vertical excitation energy.[2a]

We also evaluated the reactivity of **2** in the oxidation of hydrocarbons (Table S7). Oxidation of cyclohexane and cyclooctane by **2** under nitrogen afforded cyclohexanone and cyclooctanone in respective yields of 35% and 40%. As these products represent four-electron oxidations, their yields correspond essentially to quantitative conversion of the oxidizing equivalents from **2** present in the solution.

Second-order rate constants were measured for the reaction of **2** with substrates having different C−H bond strengths (Table S7). Figure 3 shows a plot of log k_2' ($k_2' = k_2$/number of equivalent target C−H bonds) as a function of bond dissociation energy (D_{C-H}), for which a linear correlation is seen, as previously found for other high-valent oxoiron centers. In addition, **2** exhibits C−H/D kinetic isotope effects (KIEs) of 28 and 25 for toluene and cyclohexane oxidation, respectively, showing that C−H bond cleavage is the rate-determining step (Figures S17 and S21). The nonclassical KIE values are suggestive of hydrogen tunneling effects.[12,13b]

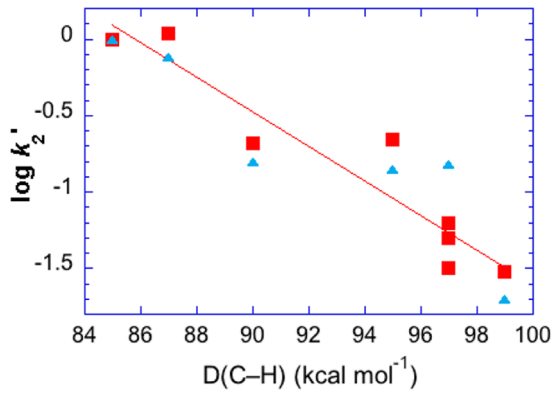

Figure 3. Plot of log k_2' values for the reactions of various substrates with **2** (squares) and $[Fe^{IV}(O)(Me_3NTB)]^{2+}$ (**3**) (triangles) at −40 °C vs their C−H bond dissociation energies ($k_2' = k_2/n$, where *n* is the number of equivalent substrate C−H bonds). See Table S7 for details.

Comparison of the HAT reactivities of **2** and other high-valent nonheme oxoiron complexes (Table S8) shows that **2** is much more reactive in cleaving C−H bonds than other well-characterized *S* = 2 $Fe^{IV}(O)$ complexes reported to date.[6,7] In fact, **2** exhibits the highest cyclohexane oxidation rate found to date for this class of complexes (k_2 = 0.37 M^{-1} s^{-1} at −40 °C). Notably, the closely related *S* = 1 $[Fe^{IV}(O)(TPA)(NCMe)]^{2+}$ complex does not react at all with cyclohexane at −40 °C. Even without correction for the temperature difference, the cyclohexane oxidation rate found for **2** at −40 °C is 3−4 orders of magnitude higher than the k_2 values at 25 °C for *S* = 1 $[Fe^{IV}(O)(N4Py)]^{2+}$ and $[Fe^{IV}(O)(BnTPEN)]^{2+}$ (N4Py = bis(2-pyridylmethyl)(bis(2-pyridyl)methyl)amine); BnTPEN = *N*-benzyl-*N*,*N*′,*N*′-tris(2-pyridylmethyl)-1,2-diaminoethane)[13b] and an order of magnitude higher than that for a recently reported $Fe^{V}(O)$ complex.[16] However, the *S* = 1 complex $[Fe^{IV}(O)(Me_3NTB)]^{2+}$ (**3**) has reactivity comparable to that of **2**, with k_2(cyclohexane) = 0.23 M^{-1} s^{-1} at −40 °C.[12] Indeed, the HAT data points for **3** (blue triangles) reported by Nam and Shaik[12] fall on the same trend line as those for **2** (red squares) in Figure 3. This surprising resemblance suggests that $Fe^{IV}(O)$ complexes, despite having different ground spin states, can achieve comparably high HAT reactivities. On the basis of DFT calculations, Nam and Shaik rationalized the high HAT reactivity of **3** by invoking a highly reactive close-lying *S* = 2 excited state.[12] More examples are needed to clarify the basis for the similar reactivities of **2** and **3** (see p S16 in the SI).

Complex **2** also epoxidizes olefins (Table S7). Although commonly associated with oxoiron(IV) porphyrin cation radical complexes,[17] olefin epoxidation has only been reported for three nonheme oxoiron(IV) complexes, in reactions limited to only one or two types of olefins.[18] Banse reported the epoxidation of cyclooctene and *cis*-stilbene in <20% yield by an $[Fe^{IV}(O)(N5)]$ complex.[18a] Rybak-Akimova found that a complex supported by a pyridine-containing tetraaza macrocycle afforded an 80% yield of cyclooctene oxide with k_2 = 0.45 M^{-1} s^{-1} at 0 °C,[18b] while Nam obtained a 60% yield of styrene oxide from $[Fe^{IV}(O)(N3S2)]^{2+}$ with k_2 = 0.03 M^{-1} s^{-1} at 25 °C.[18c] Although we initially reported the epoxidation of *cis*-cyclooctene by $[Fe^{IV}(O)(TPA)(NCMe)]^{2+}$,[10] subsequent studies with rigorous exclusion of O_2 showed no epoxide formation from cyclooctene and cyclohexene.[19] In contrast, **2** reacted with *cis*-cyclooctene at −40 °C to form epoxide in 80% yield relative to the amount of **2** present in solution. The k_2 value for cyclooctene epoxidation was determined to be 3.3 M^{-1} s^{-1} (Table S7), a value that is orders of magnitude larger than those for the *S* = 1 oxoiron(IV) complexes mentioned above (given the higher temperatures at which the latter results were obtained). These comparisons suggest a significantly higher reactivity of the *S* = 2 complex **2** toward C═C bonds than found for its *S* = 1 nonheme counterparts. However, because of the paucity of rate data for such reactions, additional examples are needed to draw firm conclusions on the role of spin state in determining the rates of olefin epoxidation.

The reactions of **2** with other olefins were investigated. The epoxidations of *cis*- and *trans*-2-heptene exhibited high degrees of stereoretention (87% and >99%, respectively), indicating that if substrate-based radical intermediates are formed, they must be short-lived. Interestingly, 1-octene was oxidized by **2** with k_2 = 5.3 M^{-1} s^{-1}; however, in this case both the epoxide and 1-octen-3-one were obtained in respective yields of 35% and 15% relative to **1**, representing 90% of the oxidizing equivalents available from **2**. On the other hand, cyclohexene oxidation by **2** afforded only allylic oxidation products. These results show that **2** can mediate the oxidation of C−H and C═C bonds at comparable rates. Indeed, the k_2 values for cyclooctene and cyclooctane oxidation

DOI: 10.1021/ja511757j
J. Am. Chem. Soc. 2015, 137, 2428−2431

by **2** are identical, indicating that **2** attacks the cyclooctene C=C bond only 16-fold faster than the 95 kcal/mol C−H bond of cyclooctane, which was confirmed by a competitive oxidation of equimolar amounts of the two substrates, which afforded 35% cyclooctene oxide and 15% cyclooctanone. These results represent the first instance for which the rates of C=C and C−H bond attack by a nonheme Fe^{IV}=O complex can be compared directly, which emphasizes the uniqueness of **2** within the nonheme oxoiron family.[20]

In summary, we have generated the highly reactive high-spin oxoiron(IV) complex **2**. Introduction of α-substituents on all three pyridines of the TPA ligand weakens the ligand field about the Fe^{IV}=O unit,[9a] and S = 1 $[Fe^{IV}(O)(TPA)(NCMe)]^{2+}$ becomes S = 2 $[Fe^{IV}(O)(TQA)(NCMe)]^{2+}$ (**2**). The Fe^{IV}=O center goes from being unreactive toward cyclohexane at −40 °C to being the fastest in its class to date at oxidizing cyclohexane. The rate of 0.37 s^{-1} at −40 °C for oxidation of 1 M cyclohexane by **2** compares favorably with the rate of 13 s^{-1} for taurine oxidation by TauD-***J*** at 5 °C, after correction for the 45° temperature difference.[2b] This observation and the strikingly similar spectroscopic parameters of **2** and TauD-***J*** (Table 1) make **2** the best electronic *and* functional model for TauD-***J*** to date.

■ ASSOCIATED CONTENT

Supporting Information

Experimental details, additional ESI-MS and Mössbauer data, DFT results and insights, kinetic data, and crystallographic data for **1** (CIF). This material is available free of charge via the Internet at http://pubs.acs.org.

■ AUTHOR INFORMATION

Corresponding Authors

*larryque@umn.edu
*emunck@cmu.edu
*eb7g@andrew.cmu.edu

Notes

The authors declare no competing financial interest.

■ ACKNOWLEDGMENTS

This work was supported by grants from the National Science Foundation (CHE-1058248 and CHE-1361773 to L.Q. and CHE-1305111 to E.M.). A.N.B. thanks the Indo-US Science & Technology Forum (IUSSTF) for a postdoctoral fellowship, and M.P. and G.T.R. thank the University of Minnesota for graduate dissertation fellowships. We thank Mr. Ang Zhou for his assistance with ^{19}F NMR experiments.

■ REFERENCES

(1) (a) Costas, M.; Mehn, M. P.; Jensen, M. P.; Que, L., Jr. *Chem. Rev.* **2004**, *104*, 939. (b) Solomon, E. I.; Brunold, T. C.; Davis, M. I.; Kemsley, J. N.; Lee, S.-K.; Lehnert, N.; Neese, F.; Skulan, A. J.; Yang, Y.-S.; Zhou, J. *Chem. Rev.* **2000**, *100*, 235.

(2) (a) Krebs, C.; Fujimori, D. G.; Walsh, C. T.; Bollinger, J. M., Jr. *Acc. Chem. Res.* **2007**, *40*, 484. (b) Price, J. C.; Barr, E. W.; Glass, T. E.; Krebs, C.; Bollinger, J. M., Jr. *J. Am. Chem. Soc.* **2003**, *125*, 13008. (c) Sinnecker, S.; Svensen, N.; Barr, E. W.; Ye, S.; Bollinger, J. M., Jr.; Neese, F.; Krebs, C. *J. Am. Chem. Soc.* **2007**, *129*, 6168.

(3) Xiao, D. J.; Bloch, E. D.; Mason, J. A.; Queen, W. L.; Hudson, M. R.; Planas, N.; Borycz, J.; Dzubak, A. L.; Verma, P.; Lee, K.; Bonino, F.; Crocellà, V.; Yano, J.; Bordiga, S.; Truhlar, D. G.; Gagliardi, L.; Brown, C. M.; Long, J. R. *Nat. Chem.* **2014**, *6*, 590.

(4) (a) Shaik, S.; Hirao, H.; Kumar, D. *Acc. Chem. Res.* **2007**, *40*, 532. (b) Decker, A.; Rohde, J.-U.; Klinker, E. J.; Wong, S. D.; Que, L., Jr.; Solomon, E. I. *J. Am. Chem. Soc.* **2007**, *129*, 15983. (c) Bernasconi, L.; Louwerse, M. J.; Baerends, E. J. *Eur. J. Inorg. Chem.* **2007**, 3023. (d) Geng, C.; Ye, S.; Neese, F. *Angew. Chem., Int. Ed.* **2010**, *49*, 5717. (e) Shaik, S.; Chen, H.; Janardanan, D. *Nat. Chem.* **2011**, *3*, 19.

(5) (a) Que, L., Jr. *Acc. Chem. Res.* **2007**, *40*, 493. (b) McDonald, A. R.; Que, L., Jr. *Coord. Chem. Rev.* **2013**, *257*, 414. (c) Ray, K.; Pfaff, F. F.; Wang, B.; Nam, W. *J. Am. Chem. Soc.* **2014**, *136*, 13942.

(6) (a) England, J.; Martinho, M.; Farquhar, E. R.; Frisch, J. R.; Bominaar, E. L.; Münck, E.; Que, L., Jr. *Angew. Chem., Int. Ed.* **2009**, *48*, 3622. (b) England, J.; Guo, Y.; Van Heuvelen, K. M.; Cranswick, M. A.; Rohde, G. T.; Bominaar, E. L.; Münck, E.; Que, L., Jr. *J. Am. Chem. Soc.* **2011**, *133*, 11880.

(7) (a) Lacy, D. C.; Gupta, R.; Stone, K. L.; Greaves, J.; Ziller, J. W.; Hendrich, M. P.; Borovik, A. S. *J. Am. Chem. Soc.* **2010**, *132*, 12188. (b) Bigi, J. P.; Harman, W. H.; Lassalle-Kaiser, B.; Robles, D. M.; Stich, T. A.; Yano, J.; Britt, R. D.; Chang, C. J. *J. Am. Chem. Soc.* **2012**, *134*, 1536.

(8) Pestovsky, O.; Stoian, S.; Bominaar, E. L.; Shan, X.; Münck, E.; Que, L., Jr.; Bakac, A. *Angew. Chem., Int. Ed.* **2005**, *44*, 6871.

(9) (a) Zang, Y.; Kim, J.; Dong, Y.; Wilkinson, E. C.; Appelman, E. H.; Que, L., Jr. *J. Am. Chem. Soc.* **1997**, *119*, 4197. (b) Paine, T. K.; Costas, M.; Kaizer, J.; Que, L., Jr. *J. Biol. Inorg. Chem.* **2006**, *11*, 272. (c) Wei, N.; Murthy, N. N.; Chen, Q.; Zubieta, J.; Karlin, K. D. *Inorg. Chem.* **1994**, *33*, 1953.

(10) Lim, M. H.; Rohde, J.-U.; Stubna, A.; Bukowski, M. R.; Costas, M.; Ho, R. Y. N.; Münck, E.; Nam, W.; Que, L., Jr. *Proc. Natl. Acad. Sci. U.S.A.* **2003**, *100*, 3665.

(11) Macikenas, D.; Skrzypczak-Jankun, E.; Protasiewicz, J. D. *J. Am. Chem. Soc.* **1999**, *121*, 7164.

(12) Seo, M. S.; Kim, N. H.; Cho, K.-B.; So, J. E.; Park, S. K.; Clémancey, M.; Garcia-Serres, R.; Latour, J.-M.; Shaik, S.; Nam, W. *Chem. Sci.* **2011**, *2*, 1039.

(13) (a) Xue, G.; De Hont, R.; Münck, E.; Que, L., Jr. *Nat. Chem.* **2010**, *2*, 400. (b) Kaizer, J.; Klinker, E. J.; Oh, N. Y.; Rohde, J.-U.; Song, W. J.; Stubna, A.; Kim, J.; Münck, E.; Nam, W.; Que, L., Jr. *J. Am. Chem. Soc.* **2004**, *126*, 472.

(14) Jackson, T. A.; Rohde, J.-U.; Seo, M. S.; Sastri, C. V.; DeHont, R.; Stubna, A.; Ohta, T.; Kitagawa, T.; Münck, E.; Nam, W.; Que, L., Jr. *J. Am. Chem. Soc.* **2008**, *130*, 12394.

(15) The ΔE_Q values were calculated using a conversion factor of −1.43 mm s^{-1}/AU instead of the conventional −1.7 mm s^{-1}/AU. See Figure 10 in: Chanda, A.; Shan, X.; Chakrabarti, M.; Ellis, W. C.; Popescu, D. L.; Tiago de Oliveira, F.; Wang, D.; Que, L., Jr.; Collins, T. J.; Münck, E.; Bominaar, E. L. *Inorg. Chem.* **2008**, *47*, 3669.

(16) Ghosh, M.; Singh, K. K.; Panda, C.; Weitz, A.; Hendrich, M. P.; Collins, T. J.; Dhar, B. B.; Gupta, S. S. *J. Am. Chem. Soc.* **2014**, *136*, 9524.

(17) (a) Meunier, B. *Chem. Rev.* **1992**, *92*, 1411. (b) Groves, J. T.; Nemo, T. E. *J. Am. Chem. Soc.* **1983**, *105*, 5786.

(18) (a) Balland, V.; Charlot, M.-F.; Banse, F.; Girerd, J.-J.; Mattioli, T. A.; Bill, E.; Bartoli, J.-F.; Battioni, P.; Mansuy, D. *Eur. J. Inorg. Chem.* **2004**, 301. (b) Ye, W.; Ho, D. M.; Friedle, S.; Palluccio, T. D.; Rybak-Akimova, E. V. *Inorg. Chem.* **2012**, *51*, 5006. (c) Annaraj, J.; Kim, S.; Seo, M. S.; Lee, Y.-M.; Kim, Y.; Kim, S.-J.; Choi, Y. S.; Nam, W. *Inorg. Chim. Acta* **2009**, *362*, 1031.

(19) (a) Mas-Ballesté, R.; Que, L., Jr. *J. Am. Chem. Soc.* **2007**, *129*, 15964. (b) Oloo, W. N.; Feng, Y.; Iyer, S.; Parmelee, S.; Xue, G.; Que, L., Jr. *New J. Chem.* **2013**, *37*, 3411.

(20) Betley has reported a high-spin iron(III)−imido radical complex that can attack olefin C−H and C=C bonds, the only other nonheme high-spin iron complex to exhibit such reactivity. See: Hennessy, E. T.; Liu, R. Y.; Iovan, D. A.; Duncan, R. A.; Betley, T. A. *Chem. Sci.* **2014**, *5*, 1526. Having more such examples will be useful for comparison.

DOI: 10.1021/ja511757j
J. Am. Chem. Soc. 2015, 137, 2428−2431